Boundary-element method for the calculation of electronic states in semiconductor nanostructures

P. A. Knipp*
Department of Physics and Computer Science, Christopher Newport University, Newport News, Virginia 23606-2998

T. L. Reinecke†
Max-Planck Institut für Festkörperforschung, Heisenbergstrasse 1, 70569 Stuttgart, Germany
and Naval Research Laboratory, Washington, D.C. 20375‡
(Received 31 January 1996)

We have developed a boundary-element method to treat the single-particle electronic properties of semiconductor nanostructures that consist of piecewise homogeneous materials of arbitrary shapes. Green's-function techniques are used to derive integral equations that determine these electronic properties. These equations involve integrals over the boundaries between the homogeneous regions, and they are discretized and solved numerically. In effect, this approach changes a partial differential equation with boundary conditions in d independent variables into an integral equation in $d-1$ independent variables, which leads to its efficiency. For bound states these methods are used to calculate eigenenergies, for scattering states to calculate differential cross sections, and for both bound and scattering states to calculate spectral density functions and wave functions. For such systems, we show that this method generally provides improved calculational efficiency as compared to alternative approaches such as plane-wave expansions, finite-difference methods, or finite-element methods and that it is more effective in treating highly excited states than are these methods. Illustrative examples are given here for several systems whose potentials are functions of two variables, such as quantum wires or patterned two-dimensional electron gases. [S0163-1829(96)09227-2]

I. INTRODUCTION

Quantum wires, quantum dots, and other more complex structures that involve confinement in more than one dimension are of considerable current interest. Such structures are being produced in a variety of ways including growth as microcrystals, in nonequilibrium growth such as molecular-beam epitaxy, formation by lithography and etching, and by the use of chemical and biological templates and processes. Perhaps the most intensely investigated materials involve semiconductors, but other materials including insulators and metals are also being studied. These systems permit the investigation of different physical phenomena in effectively one and zero dimensions. From a technological point of view, such structures are of interest because of their potential for future advanced technologies such as highly integrated electronic and optical systems.

In order to obtain a full understanding of these systems and to provide a detailed interpretation of experimental results for realistic systems it is necessary to have quantitative results for the single-particle electronic states of such structures. In the case of quantum wells and superlattices, Schrödinger's equation generally separates, and such results can readily be obtained from one-dimensional calculations. For lower-dimensional structures Schrödinger's equation generally does not separate; to date either simple approximations or numerically extensive methods have been used. In the present work we present a numerical approach for calculating quantitatively the single electronic properties of low-dimensional structures of general shape that is relatively efficient and conveniently gives results for high-lying and for continuum states.

For a few examples of highly symmetrical structures such as cylindrical wires or spherical dots, Schrödinger's equation is separable, meaning that any wave function $\psi(\mathbf{r})$ can be written in the form $\psi(\mathbf{r})=f(\eta)g(\zeta)h(\xi)$, where (η,ζ,ξ) are some appropriate set of curvilinear coordinates, and $E=E_i^{(\eta)}+E_j^{(\zeta)}+E_k^{(\xi)}$, where the three terms on the right-hand side are eigenenergies associated with the motion along the individual spatial coordinates. However, most realistic systems of physical interest are not of such simple shapes, and their wave functions and energies are nonseparable. Physically, the reasons that such equations are not in general separable are that (i) the potential in Schrödinger's equation may not be written as a simple sum of potentials each dependent on a single variable, or (ii) the boundary conditions on the wave functions in lower-dimensional systems involve more than one of the variables. Thus numerical techniques must be used to study the properties of such realistic structures.

Some numerical techniques which are used for studying such semiconductor nanostructures include plane-wave expansions,[1] finite-difference methods,[2] and finite-element methods.[3] Plane-wave expansions are found to converge relatively slowly in the vicinity of the interfaces of nanostructures where the potentials change rapidly. Finite-difference methods involve discretizing Schrödinger's equation in the two (or more) variables that do not separate. The resulting matrix to be diagonalized then increases roughly with the product of the numbers of points chosen in each direction and can involve relatively large matrices. Finite-element methods bear a resemblance to finite-difference methods. Each of these methods has difficulties in treating highly excited or continuum states, for which the wave functions vary rapidly over the nanostructure.

Here we present an alternative method that is efficient and

TABLE I. Green's functions for uniform regions having one, two, or three independent variables, where $H_0^{(1)}$ is the zeroth-order Hankel function of the first kind and K_0 is a zeroth-order modified Bessel function. In the classically allowed regions $k^2 \equiv 2m(E-\mathcal{V})/\hbar$ and in the classically forbidden regions $\gamma^2 \equiv 2m(\mathcal{V}-E)/\hbar$.

Number of independent variables	Classically allowed ($E>\mathcal{V}$)	Classically forbidden ($E<\mathcal{V}$)	Form of small-r divergence
1	$\frac{ie^{ik\|x\|}}{2k}$	$\frac{e^{-\gamma\|x\|}}{2\gamma}$	none
2	$\frac{iH_0^{(1)}(kr)}{4}$	$\frac{K_0(\gamma r)}{2\pi}$	$-\frac{\ln r}{2\pi}$
3	$\frac{e^{ikr}}{4\pi r}$	$\frac{e^{-\gamma r}}{4\pi r}$	$\frac{1}{4\pi r}$

straightforward for the calculation of the wave functions, eigenenergies, scattering cross sections, and spectral density functions of electrons in arbitrarily shaped nanostructures composed of different uniform regions. It is called the ''boundary-element method'' and we show that it provides advantages, including improved numerical efficiency, over alternate approaches. In previous work we have used a similar method to treat the LO phonons of quantum wire[4] and quantum dot[5] structures and we have also developed such methods to treat photons[6] and acoustic phonons[7] in heterostructures. Here we develop and discuss this method for electrons in such systems. For the present purpose we use the effective-mass approximation for the electrons. In general, electron, phonon, or photon states are determined by a partial differential equation, whose solution satisfies certain boundary conditions. For the cases of a wave confined to or excluded from a region of finite spatial extent it is known[8] that by using Green's-function techniques one may transform the system of a differential equation and boundary conditions into an integral equation over only the internal interface(s) of the system; these equations can then be discretized and solved numerically.[9] Here we extend this technique to inhomogeneous systems such as semiconductor heterostructures, which involve the quantum-mechanical motion of an electron from one homogeneous region to another.

The formalism that we will present is valid in nanostructure systems that have quasi-two-dimensional geometry such as quantum wells or superlattices, quasi-one-dimensional geometry such as quantum wires, or quasi-zero-dimensional geometry such as quantum dots. For the sake of illustration, we will limit our examples to cases of systems that have potential variations in two dimensions in order to demonstrate most simply the effects of nonseparability and nonintegrability. Such results can be considered to apply to at least two otherwise dissimilar classes of nanostructures: (i) quantum wires, which have translational symmetry in the one direction, and (ii) heterojunctions or quantum wells that have been laterally patterned to create quantum dots whose vertical extent is so much smaller than its lateral extent that the vertical motion essentially decouples from the in-plane motion.

In Sec. II the basic equations used for the subsequent development are written down. In Secs. III–V we use these equations to develop the boundary-element method for the electronic states in various parts of the energy spectrum. In Sec. III we do this for the discrete part of the spectrum and we give results for the energies and wave functions of the bound states. In Sec. IV we treat the continuum portion of the spectrum, calculating differential scattering cross sections for the case of incident plane waves. In Sec. V we calculate spectral density functions, which offer a unified representation of electronic states in all portions of the spectrum, both discrete and continuum. In Sec. VI we will give examples of all of these physical quantities for several shapes and systems which depend on two variables.

II. FORMALISM

Within the effective-mass approximation[10] Schrödinger's equation can be written in the form

$$\left[-\frac{\hbar^2}{2}\nabla\cdot m(\mathbf{r})^{-1}\nabla+\mathcal{V}(\mathbf{r})-E\right]\psi(\mathbf{r})=0, \tag{1}$$

where the carrier mass $m(\mathbf{r})$ and the band offset $\mathcal{V}(\mathbf{r})$ are piecewise uniform, i.e., are constants in the several regions of the nanostructure.[11] Across an interface separating two different regions, both the wave function ψ and its inverse-mass weighted normal derivative are continuous. If there is no magnetic field, the Hamiltonian is time reversible and the wave functions can be expressed as real quantities. Within a particular region V of the nanostructure through which m and $\mathcal{V}$ are uniform, the equation governing the Green's function is

$$\left[-\nabla^2+\frac{2m}{\hbar^2}(\mathcal{V}-E)\right]G(\mathbf{r},\mathbf{r}';E)=\delta(\mathbf{r}-\mathbf{r}'), \tag{2}$$

where E is complex (usually with only a small imaginary component). Following the usual convention, the particular (and unique) form chosen for G satisfies $\lim_{|\mathbf{r}-\mathbf{r}'|\to\infty}G(\mathbf{r},\mathbf{r}';E)=0$ if $\mathrm{Im}(E)>0$. For uniform regions [where $m(\mathbf{r})$ and $\mathcal{V}(\mathbf{r})$ are constants] the results for the Green's function are listed in Table I for various geometries.

In Table I and in the following development we find it convenient to discuss issues in terms of the number of independent variables that need to be treated numerically in the problem under consideration. Typically this number is that of the largest set of variables that do not separate from one another in the problem. For example, in the case of a quantum well, the motion along the growth direction separates from the motion in the plane of the well and this latter two-dimensional motion separates into independent one-dimensional motions owing to translational symmetry. The

variable of interest here is usually along the growth direction. In the case of quantum wire the motion along the wire axis separates from the motion in the transverse directions and 2 is the number of independent variables that do not separate. In the case of patterned two-dimensional systems, whose lateral extent typically greatly exceeds their vertical extent [$=O(5\ \text{nm})$], the mismatch of the sizes ensures that the motion in the growth direction separates from that in the transverse directions owing to the symmetry-breaking induced by the patterning process. The motion in the two transverse directions generally do not separate from one another, leading also to 2 as the number of independent variables that are not separable. For a quantum dot that has no symmetry axis and for which all three orthogonal spatial lengths are of the same order of magnitude, 3 is the number of independent variables that must be treated simultaneously. Correspondingly, in Table I the Green's functions for the number of independent Cartesian variables involved are listed. These Green's functions correspond essentially to free motion in one-, two-, or three-dimensional space.

III. $E<0$: BOUND-STATE ENERGIES AND WAVE FUNCTIONS

We begin by multiplying Eq. (1) by $2mG(\mathbf{r},\mathbf{r}';E)/\hbar^2$ and subtracting the resulting equation from Eq. (2) multiplied by $\psi(\mathbf{r})$, where $\mathbf{r}$ and $\mathbf{r}'$ are within V, a particular region throughout which the material properties are uniform. Integrating the resulting equation over $\mathbf{r}$ through the volume V and using Green's theorem, we obtain

$$\int_S d\mathbf{A}[m\phi(\mathbf{A})G(\mathbf{A},\mathbf{r}';E)-\psi(\mathbf{A})\partial_{\mathbf{A}}G(\mathbf{r},\mathbf{r}';E)]=\psi(\mathbf{r}'), \tag{3}$$

where S is the surface bounding V, $\mathbf{A}$ indicates a point $\mathbf{r}_{\mathbf{A}}$ located on S, $\phi(\mathbf{A})\equiv m^{-1}\partial_{\mathbf{A}}\psi(\mathbf{r})$, $\partial_{\mathbf{A}}\equiv\hat{n}_{\mathbf{A}}\cdot\partial/\partial\mathbf{r}|_{\mathbf{A}}$, and $\hat{n}_{\mathbf{A}}$ is the normal vector that points *out* of the region V at the point $\mathbf{A}$. Note that the reason for the m^{-1} factor in our definition for ϕ is so that ϕ is single valued, modulo a minus sign, at the interface. It is seen from Eq. (3) that if one has values for (i) the Green's function everywhere within V, (ii) the wave function at all points $\mathbf{A}$ on the surface S, and (iii) the (inner) normal derivative of the wave function for all $\mathbf{A}\in S$, then one can calculate ψ everywhere within V. In order to calculate $\psi(\mathbf{A})$ and $\phi(\mathbf{A})$ we evaluate Eq. (3) at a point $\mathbf{r}'$ that is within V but arbitrarily close to S and we interchange $\mathbf{A}$ and $\mathbf{A}'$ to obtain the homogeneous integral equation

$$\int_S d\mathbf{A}'[B(\mathbf{A},\mathbf{A}')\phi(\mathbf{A}')+C(\mathbf{A},\mathbf{A}')\psi(\mathbf{A}')]=0 \tag{4}$$

where the kernels are given by $B(\mathbf{A},\mathbf{A}')\equiv 2mG(\mathbf{A},\mathbf{A}';E)$ and $C(\mathbf{A},\mathbf{A}')\equiv -2\partial_{\mathbf{A}'}G(\mathbf{r}',\mathbf{A};E)-\delta(\mathbf{A}-\mathbf{A}')$. It should be noted that for the piecewise uniform nanostructures considered here the Green's functions involved in Eqs. (3) and (4) are known straightforwardly and are given in Table I.

If the composite system consists of N different homogeneous regions, then such an integral equation can be derived for each of the N regions, including both classically allowed and classically forbidden regions, as well as regions of either finite or infinite spatial extent. Because $G(\mathbf{r},\mathbf{r}';E)$ vanishes as either r or r' goes to infinity, the ''surface'' at infinity does not appear in any of these equations. The entire linear system of integral equations can then be represented as

$$\begin{bmatrix}0\\0\\\vdots\\0\end{bmatrix}=\begin{bmatrix}B_1 & C_1\\B_2 & C_2\\\vdots & \vdots\\B_N & C_N\end{bmatrix}\begin{bmatrix}\phi\\\psi\end{bmatrix}\equiv M\begin{bmatrix}\phi\\\psi\end{bmatrix}, \tag{5}$$

where B_I and C_I represent the Ith region's integral operators, which depend parametrically on the energy E. The lower half of the (symbolic) column vector $\left[\begin{smallmatrix}\phi\\\psi\end{smallmatrix}\right]$ contains the values of the wave function on all interfaces, and the upper half contains the values of the normal derivatives of the wave function divided by the effective mass m. If the particle's motion is classically forbidden in all regions of infinite spatial extent and is classically allowed in at least one of the finite regions, then the energy spectrum contains a bound portion. The energies of these bound states are determined by finding the nontrivial solutions of Eq. (5), which occur for certain discretely spaced (real) values of E.

A number of ways exist to solve Eq. (5) numerically. We choose to do this by using what is known as the boundary-element method (BEM). To implement this approach we discretize the integral in Eq. (4), thus approximating it as a sum of n terms, to obtain

$$\sum_{j=1}^{n}(B_{ij}\phi_j+C_{ij}\psi_j)=0, \tag{6}$$

where $B_{ij}\equiv\int_j d\mathbf{A}'B(\mathbf{A}_i,\mathbf{A}')$, $C_{ij}\equiv\int_j d\mathbf{A}'C(\mathbf{A}_i,\mathbf{A}')$, $\phi_j\equiv\phi(\mathbf{A}_j)$, $\psi_j\equiv\phi(\mathbf{A}_j)$, and $\int_j$ represents the integration over a small boundary element S_j, where $\Sigma_{j=1}^{n}S_j=S$, and n is the number of boundary elements on S. The entire set of homogeneous integral equations then is approximated by a homogeneous equation represented again by Eq. (5), but for which B_I and C_I are $n_I\times\mathcal{N}$ matrices (instead of integral operators), M is a $2\mathcal{N}\times 2\mathcal{N}$ matrix (instead of an integral operator), ϕ and ψ are $\mathcal{N}$-component column vectors (instead of functions), and $\mathcal{N}\equiv\frac{1}{2}\Sigma_{I=1}^{N}n_I$, where n_I is the number of boundary elements on S_I, the surface of the Ith region. The divisor of 2 in the definition of $\mathcal{N}$ originates from the fact that each boundary element serves two different regions.

The discretized version of Eq. (5) will have a nontrivial solution only if the determinant of the complex-valued matrix M vanishes. For the bound states, this determinant vanishes for values of E that are discretely spaced in the complex plane. We usually find these energies to be slightly removed from the real axis owing to the approximation associated with discretizing the integral equation. This procedure yields accurate results for the energies of those bound states for which the wave functions, or, more precisely, the wave functions and their normal derivatives evaluated along the boundary S, vary slowly on the scale of a typical boundary element. In order accurately to determine highly excited states the grid of boundary elements needs to be sufficiently fine.

A few technical points about the implementation of the BEM are worth mentioning. For the case of three independent variables the singularity in the Green's function causes the kernels $B(\mathbf{A},\mathbf{A}')$ and $C(\mathbf{A},\mathbf{A}')$ to diverge as $|\mathbf{r_A}-\mathbf{r_{A'}}|^{-1}$. For the case of two independent variables, B diverges logarithmically as $\mathbf{A}\rightarrow\mathbf{A}'$ and C approaches a number proportional to the local radius of curvature. For smooth surfaces these singularities are integrable in the sense that $\lim_{\delta\rightarrow\varnothing}\int_\delta d\mathbf{A}|\mathbf{A}-\mathbf{A}'|^{-1}\rightarrow 0$, even if $\mathbf{A}'\in\delta\subset S$. For nonsmooth surfaces (i.e., those having cusps, corners, or edges) these singularities are nonintegrable. For the case of an electron completely confined to or excluded from a region, this nonintegrability leads to divergent values of $\phi(A)$ near the nonsmooth singularity,[12] and for the case of interface optical-phonon modes near such singularities, a similar nonintegrability causes qualitative changes in the frequency spectrum.[4,5] For the case considered here, namely, that of electrons that are allowed to tunnel into classically forbidden regions, no such qualitative difficulties are encountered.

After calculating a particular eigenenergy E_p by standard rootfinding methods, the column-vector components ϕ_j and ψ_j are determined by finding the null eigenvector of the square matrix. The (unnormalized) wave function is then calculated by discretizing Eq. (3) to obtain

$$\psi(\mathbf{r}')=\sum_j\left[m\phi_j\int_j d\mathbf{A}G(\mathbf{A},\mathbf{r}';E_p)-\psi_j\int_j d\mathbf{A}\partial_{\mathbf{A}}G(\mathbf{r},\mathbf{r}';E_p)\right]. \tag{7}$$

We conclude this section by mentioning how the equations derived in it are modified to treat the special case studied in earlier work of a wave that is completely confined to a nanostructure. In this case, the boundary condition satisfied by the wave function is that $\psi(\mathbf{A})$ vanishes. Hence Eq. (3) is modified by setting $\psi(\mathbf{A})$ to vanish, Eq. (4) by setting $\psi(\mathbf{A}')$ to vanish, and Eqs. (6) and (7) by setting ψ_j to vanish. Equation (5) is replaced by the integral equation $B\phi=0$.

IV. $E>0$: SCATTERING CROSS SECTION

Consider a nanostructure that consists of several regions, only one (the Nth) of which extends to infinity. If $\mathcal{V}=0$ in this region, then $E>0$ represents the continuous portion of the energy spectrum, which corresponds to delocalized states. For these states one is often interested in the differential scattering cross section. If an incoming electron having momentum $\hbar\mathbf{k}$ impinges upon the nanostructure, the wave scatters elastically into other plane-wave states. In the Nth region, asymptotically far from the other regions, the wave function will have the forms

$$\psi=\begin{cases} e^{ikx}+Re^{-ikx}, & \text{one dimension,} \quad x<0 \\ Te^{ikx}, & \text{one dimension,} \quad x>0 \\ e^{i\overline{k_i}\cdot\overline{r}}+f(\theta,\overline{k_i})\dfrac{e^{ikr}}{\sqrt{r}}, & \text{two dimensions} \\ e^{i\mathbf{k}_i\cdot\mathbf{r}}+f(\hat{\mathbf{k}}_f,\mathbf{k}_i)\dfrac{e^{ikr}}{r}, & \text{three dimensions,} \end{cases} \tag{8}$$

where $f(\theta,\overline{k_i})$ and $f(\hat{\mathbf{k}}_f,\mathbf{k}_i)$ are the angle-dependent differential amplitudes for elastic scattering in two- and three-dimensions, R and T are the reflection and transmission coefficients for scattering in one dimension, $\overline{k_i}$ and $\mathbf{k}_i$ are the electron's initial wave vector in two and three dimensions, $\mathbf{k}_f$ is the electron's final vector in three dimensions, θ is the angle of the electron's final motion in the two-dimensional case, and $k\equiv|\mathbf{k}_i|=|\mathbf{k}_f|=|\overline{k_i}|=|\overline{k_f}|$. In two and three dimensions the differential scattering cross section is $|f|^2$. For a wire geometry, $|f|^2$ is the differential scattering cross section per unit length of the wire.

For all regions except for the Nth one, Eqs. (3) and (4) are valid. In the Nth region we have a formula that differs slightly from Eq. (3):

$$\psi(\mathbf{r}')=e^{i\mathbf{k}\cdot\mathbf{r}'}+\int_{S_N}d\mathbf{A}[m[\phi(\mathbf{A})-\phi_0(\mathbf{A})]G(\mathbf{A},\mathbf{r}';E)-[\psi(\mathbf{A})-\psi_0(\mathbf{A})]\partial_{\mathbf{A}}G(\mathbf{r},\mathbf{r}';E)], \tag{9}$$

where S_N consists of the finite surface separating V_N from the other $(N-1)$ regions, but does not include the surface at infinity,

$$\psi_0(\mathbf{A})\equiv e^{i\mathbf{k}\cdot\mathbf{r_A}}\begin{cases}1, & \mathbf{A}\in S_N \\ 0, & \mathbf{A}\notin S_N\end{cases} \tag{10}$$

and

$$\phi_0(\mathbf{A})\equiv\frac{e^{i\mathbf{k}\cdot\mathbf{r_A}}}{m}\begin{cases}i\mathbf{k}\cdot\hat{\mathbf{n}}_{\mathbf{A}}, & \mathbf{A}\in S_N \\ 0, & \mathbf{A}\notin S_N.\end{cases} \tag{11}$$

When the limit is taken as $\mathbf{r}'\rightarrow\mathbf{A}'$ in Eq. (9), an inhomogeneous integral equation for $\phi(\mathbf{A})$ and $\psi(\mathbf{A})$ is obtained:

$$\int_{S_N}d\mathbf{A}'[B(\mathbf{A},\mathbf{A}')\phi(\mathbf{A}')+C(\mathbf{A},\mathbf{A}')\psi(\mathbf{A}')]=\int_{S_N}d\mathbf{A}'[B(\mathbf{A},\mathbf{A}')\phi_0(\mathbf{A}')+C(\mathbf{A},\mathbf{A}')\psi_0(\mathbf{A}')], \tag{12}$$

where the kernels B and C are the same as defined in Sec. III. When this is combined with the other $(N-1)$ regions' homogeneous integral equations, which are of the same form as Eq. (4), the resulting inhomogeneous system of equations governing $\begin{bmatrix}\phi\\ \psi\end{bmatrix}$ is

$$M\begin{bmatrix}\phi\\ \psi\end{bmatrix}=M_0\begin{bmatrix}\phi_0\\ \psi_0\end{bmatrix}, \tag{13}$$

where the integral operator M is the same as that appearing in Eq. (5), and

$$M_0\equiv\begin{bmatrix}0 & 0\\ \vdots & \vdots\\ 0 & 0\\ B_N & C_N\end{bmatrix}. \tag{14}$$

Unlike Eq. (5), Eq. (13) is inhomogeneous.

We solve Eq. (13) numerically in the same way as for Eq. (5), by discretizing and using the BEM. The discretized form of Eq. (12) is

$$\sum_{j=1}^{n} (B_{ij}\phi_j + C_{ij}\psi_j) = \sum_{j=1}^{n} (B_{ij}\phi_j^{(0)} + C_{ij}\psi_j^{(0)}), \qquad (15)$$

$\psi_j^{(0)} \equiv \psi_0(\mathbf{A}_j)$, $\phi_j^{(0)} \equiv \phi_0(\mathbf{A}_j)$, and where B_{ij}, C_{ij}, ϕ_j, and ψ_j are the same as those defined in Sec. III. Hence the entire set of integral equations is then approximated by an inhomogeneous equation represented by Eq. (13), but for which M and M_0 are $2\mathcal{N}\times 2\mathcal{N}$ matrices and $\left[\begin{smallmatrix}\phi_0\\ \psi_0\end{smallmatrix}\right]$ is a $2\mathcal{N}$-component column vector. This equation is then solved by matrix inversion:

$$\begin{bmatrix}\phi\\ \psi\end{bmatrix} = M^{-1}M_0\begin{bmatrix}\phi_0\\ \psi_0\end{bmatrix}. \qquad (16)$$

In three dimensions the differential scattering amplitude is obtained by equating Eq. (8) with the large-r' form of Eq. (9) to obtain

$$f(\hat{\mathbf{k}}_f, \mathbf{k}_i) = \frac{1}{4\pi}\int_{S_N} d\mathbf{A} e^{-i\mathbf{k}_f\cdot\mathbf{r}_\mathbf{A}}\{m[\phi(\mathbf{A}) - \phi_0(\mathbf{A})] + i\mathbf{k}_f\cdot\hat{\mathbf{n}}_\mathbf{A}[\psi(\mathbf{A}) - \psi_0(\mathbf{A})]\}. \qquad (17)$$

In two dimensions this formula is unchanged, except that the $1/4\pi$ prefactor is replaced by $1 + i/4\sqrt{\pi k}$ owing to the asymptotic behavior of the Bessel function and that the integral over the closed surface S_N is replaced by an integral over a closed contour. In one dimension, the reflection (R) and transmission (T) coefficients are trivially related to the values of the wave function ψ evaluated at the left and right boundaries of the nanostructure.

Now we describe how the equations derived in this section are modified to treat the special case studied in previous work of a wave that is completely excluded from a nanostructure, for which the boundary condition satisfied by the wave function is that $\psi(\mathbf{A})$ vanishes. Hence Eqs. (9) and (17) are modified by setting $\psi(\mathbf{A})$ to vanish, Eq. (12) by setting $\psi(\mathbf{A}')$ to vanish, and Eq. (15) by setting ψ_j to vanish. Equations (13), (14), and (16) are replaced by the single integral equation $B\phi = B\phi_0 + C\psi_0$. Equations (8), (10), and (11) are not modified at all.

V. $E<0$ OR $E>0$: SPECTRAL DENSITY FUNCTION

A very useful way to present results for the discrete and continuous portions of the spectrum in a unified way is through the use of the spectral density function $\Sigma_\nu \psi_\nu(\mathbf{r})\psi_\nu(\mathbf{r}')^*\delta(E - E_\nu)$, where all states of the system are included in the sum over ν, in which E_ν and ψ_ν are the energy and normalized wave function of the νth state. In cases where there is no magnetic field, the Hamiltonian is time reversible and the wave functions $\psi_\nu(\mathbf{r})$ can be expressed as purely real quantities. The spectral density function is a purely real quantity that is symmetric in $\mathbf{r}$ and $\mathbf{r}'$. For $\mathbf{r} = \mathbf{r}'$ the spectral density function is useful in providing a picture of the spatial dependence of the density of states, including both the discrete and continuous portions of the spectrum. In addition, this representation eliminates ambiguities associated with degeneracies. In the continuum, for instance, the states are usually infinitely degenerate and then it is more relevant when discussing physical quantities to consider the spectral density at a particular energy rather than one of the degenerate wave functions at that energy. In previous work[13] we have found the corresponding spectral densities for optical phonons to be useful in picturing the vibrational amplitudes' spatial dependence and in representing the results of electron-phonon scattering.[13]

Often it is convenient to represent the spectral density function as $\pi^{-1}\lim_{\mathrm{Im}(E)\to 0^+}\mathrm{Im}[\rho(\mathbf{r},\mathbf{r}';E]$, where the complex-valued spectral density function $\rho(\mathbf{r},\mathbf{r}';E)$ is defined by

$$\rho(\mathbf{r},\mathbf{r}';E) = \sum_\nu \frac{\psi_\nu(\mathbf{r})\psi_\nu^*(\mathbf{r}')}{E_\nu - E}. \qquad (18)$$

It is straightforward to verify that the complex-valued spectral density function ρ satisfies the equation

$$\left[-\frac{\hbar^2}{2}\nabla\cdot m(\mathbf{r})^{-1}\nabla + \mathcal{V}(\mathbf{r}) - E\right]\rho(\mathbf{r},\mathbf{r}';E) = \delta(\mathbf{r}-\mathbf{r}'). \qquad (19)$$

For small $|\mathbf{r}-\mathbf{r}'|$, for large E, or for a homogeneous system, the spectral density ρ equals $2mG(\mathbf{r},\mathbf{r}';E)/\hbar^2$.

In the following we will not explicitly indicate the E dependence of the spectral density and of the Green's function. We multiply Eq. (19) evaluated at $(\mathbf{r},\mathbf{r}'')$ by $2mG(\mathbf{r},\mathbf{r}')/\hbar^2$ and subtract the resulting equation from Eq. (2) multiplied by $\rho(\mathbf{r},\mathbf{r}'')$, where the points $\mathbf{r}$, $\mathbf{r}'$, and $\mathbf{r}''$ are in the region V. Then we integrate the resulting equation over $\mathbf{r}$ over the volume V and use Green's theorem to obtain

$$\int_S d\mathbf{A}[G(\mathbf{A},\mathbf{r}')\partial_\mathbf{A}\rho(\mathbf{r},\mathbf{r}'') - \rho(\mathbf{A},\mathbf{r}'')\partial_\mathbf{A}G(\mathbf{r},\mathbf{r}')] = \rho(\mathbf{r}',\mathbf{r}'') - 2mG(\mathbf{r}'',\mathbf{r}')/\hbar^2. \qquad (20)$$

Thus having values for $\partial_\mathbf{A}\rho(\mathbf{r},\mathbf{r}'')$ and $\rho(\mathbf{A},\mathbf{r}'')$ enables one to calculate $\rho(\mathbf{r}',\mathbf{r}'')$ for all $\mathbf{r}'$ within V. To calculate the former two quantities, we carefully take the limit as $\mathbf{r}''\to\mathbf{A}''$ in Eq. (20), which yields

$$\int_S d\mathbf{A}[G(\mathbf{A},\mathbf{r}')m\Pi(\mathbf{A},\mathbf{A}'') - \rho(\mathbf{A},\mathbf{A}'')\partial_\mathbf{A}G(\mathbf{r},\mathbf{r}')] = \rho(\mathbf{r}',\mathbf{A}'') - mG(\mathbf{A}'',\mathbf{r}')/\hbar^2, \qquad (21)$$

where $\Pi(\mathbf{A},\mathbf{A}'') \equiv m^{-1}\partial_\mathbf{A}\rho(\mathbf{r},\mathbf{A}'')$. Thus having values for $\rho(\mathbf{A},\mathbf{A}'')$ and $\Pi(\mathbf{A},\mathbf{A}'')$ enables one to calculate $\rho(\mathbf{r}',\mathbf{A}'')$ for all $\mathbf{r}'$ within V.

To calculate $\rho(\mathbf{A},\mathbf{A}')$ and $\Pi(\mathbf{A},\mathbf{A}')$ we evaluate Eq. (21) at a point $\mathbf{r}'$ that is within V but very close to S. This yields the integral equation

$$\int_S d\mathbf{A}'[B(\mathbf{A},\mathbf{A}')\Pi(\mathbf{A}',\mathbf{A}'') + C(\mathbf{A},\mathbf{A}')\rho(\mathbf{A}',\mathbf{A}'')] = -2mG(\mathbf{A},\mathbf{A}'')/\hbar^2, \qquad (22)$$

where for convenience we have made the interchange of variable $\mathbf{r}'\leftrightarrow\mathbf{r}$. Performing the above procedure in all N

regions of the nanostructure yields the inhomogeneous system of linear integral equations

$$M\begin{bmatrix}\Pi\\ \rho\end{bmatrix}=-\hbar^{-2}\begin{bmatrix}B_1\\ B_2\\ \vdots\\ B_N\end{bmatrix}, \tag{23}$$

where the integral operator M is the same as that appearing in Eqs. (5) and (13). Unlike Eqs. (5) and (13), in which the upper and lower halves of the column vector $\left[\begin{smallmatrix}\phi\\ \psi\end{smallmatrix}\right]$ are functions of one variable $(\mathbf{A})$, the upper and lower halves of the column vector $\left[\begin{smallmatrix}\pi\\ \rho\end{smallmatrix}\right]$ in Eq. (23) are functions of two variables $(\mathbf{A},\mathbf{A}')$. Unlike Eq. (5) and like Eq. (13), Eq. (23) is inhomogeneous.

We solve Eq. (23) numerically in the same way as for Eqs. (5) and (13), using the BEM. The discretized form of Eq. (22) is

$$\sum_{j=1}^{n}(B_{ij}\Pi_{jk}+C_{ij}\rho_{jk})=-B_{ik}/\hbar^2, \tag{24}$$

where $\Pi_{ij}\equiv\int_j d\mathbf{A}'\,\Pi(\mathbf{A}_i,\mathbf{A}')$, $\rho_{ij}\equiv\int_j d\mathbf{A}'\,\rho(\mathbf{A}_i,\mathbf{A}')$, and n again is the number of boundary elements on the surface S. The linear system of inhomogeneous integral equations then is approximated by

$$M\begin{bmatrix}\Pi\\ \rho\end{bmatrix}=-\hbar^{-2}\begin{bmatrix}B_1\\ B_2\\ \vdots\\ B_N\end{bmatrix}\equiv Y, \tag{25}$$

where M is a $2\mathcal{N}\times 2\mathcal{N}$ matrix (as opposed to an integral operator), Π and ρ are $\mathcal{N}\times\mathcal{N}$ matrices (as opposed to functions of two variables), B_I are $n_I\times\mathcal{N}$ matrices (instead of functions of two variables), m_I is the effective mass in the Ith region, and Y is a $2\mathcal{N}\times\mathcal{N}$ matrix. Equation (25) is solved by matrix inversion

$$\begin{bmatrix}\Pi\\ \rho\end{bmatrix}=M^{-1}Y. \tag{26}$$

When $\mathrm{Im}(E)\to 0$ and E is in the bound portion of the spectrum, $\left[\begin{smallmatrix}\Pi\\ \rho\end{smallmatrix}\right]$ diverges when $\det(M)$ vanishes (i.e., for $E=E_\nu$) and $\left[\begin{smallmatrix}\Pi\\ \rho\end{smallmatrix}\right]$ is purely real when $\det(M)$ does not vanish. Away from the bound portion of the spectrum, the imaginary part of the spectral density is a continuous nonzero function of E. When E is analytically continued into the complex plane near the bound portion of the spectrum, this gives rise to Lorentzians in the spectral density whose width in E is proportional to $\mathrm{Im}(E)$.

For each value of E, the column vector $\left[\begin{smallmatrix}\Pi\\ \rho\end{smallmatrix}\right]$ contains $2\mathcal{N}^2$ numbers. Instead of using Eqs. (20) and (21) to generate $\rho(\mathbf{r},\mathbf{r}';E)$ from $\rho(\mathbf{A},\mathbf{A}';E)$ and $\Pi(\mathbf{A},\mathbf{A}';E)$, it is usually convenient for purposes of display and of analysis to condense these data by looking at a function of the single variable E. One possible function to look at is $\int_S\int_S d\mathbf{A}d\mathbf{A}'g(\mathbf{A},\mathbf{A}')\mathrm{Im}[\rho(\mathbf{A},\mathbf{A}';E)]$, where $g(\mathbf{A},\mathbf{A}')$ is an arbitrary weighting function, which we usually choose to equal $\delta(\mathbf{A}-\mathbf{A}')$. This provides a picture of the density of states in the vicinity of the nanostructure. For a homogeneous material or for large E, this yields a function proportional to $E^{d/2-1}$, owing to the density of states of an electron in d-dimensional free space. Because of degeneracy-induced ambiguities discussed earlier regarding continuum states, there is some flexibility involved in the construction of a wave function for a fixed value of E (>0). The most general form for the $\mathbf{r}$ dependence of a (unnormalized) wave function of such a state at energy E is given by

$$\int_S d\mathbf{A}''f(\mathbf{A}'')\mathrm{Im}\Bigg[\int_S d\mathbf{A}'[G(\mathbf{r},\mathbf{A}';E)\Pi(\mathbf{A}',\mathbf{A}'';E) -\rho(\mathbf{A}',\mathbf{A}'';E)\partial_{\mathbf{A}'}G(\mathbf{r},\mathbf{r}';E)]+G(\mathbf{A}'',\mathbf{r};E)/2\Bigg], \tag{27}$$

where $f(\mathbf{A})$ is another arbitrary weighting function, which we usually choose to be a constant.

TABLE II. Convergence of the BEM-calculated energies of the ground (E_0) and first excited (E_1) states of a 25×50 nm^2 stadium-shaped dot for which $m_1=m_2=0.0665$ and the band offset is 10 meV as a function of $\mathcal{N}$, the number of boundary elements in the irreducible surface.

$\mathcal{N}$	E_0	E_1
4	$4.8823-0.1200i$	$8.7019-0.0373i$
8	$4.8095+0.0008i$	$8.6614-0.0223i$
16	$4.8042+0.0006i$	$8.6403-0.0076i$
32	$4.8028+0.0002i$	$8.6334-0.0022i$
64	$4.8024+0.0001i$	$8.6312-0.0005i$
128	$4.8023+0.0000i$	$8.6308-0.0002i$

VI. EXAMPLES

In this section we give results of calculations of the electronic properties of several model systems using the BEM discussed above. For the purpose of verifying the correctness and accuracy of the present method, we have studied a number of separable systems such as circular quantum dots, and in the large-$\mathcal{N}$ limit we have found complete agreement between BEM results and those obtained by analytical methods. Rather than produce the details of those studies here, we present instead results for nonseparable systems that illustrate the kinds of results obtainable and the characteristics of the calculations. The systems chosen are also typical of problems of current physical interest. For simplicity, we choose these systems to be characterized by two nonseparable variables as described in connection with Table I.

A. Stadium

In Table II and Figs. 1–3 we give results for a ''stadium'' shape of size 25×50 nm^2 sketched in Figs. 1 and 2. The stadium's perimeter consists of two straight line segments and two semicircles. This shape has been studied theoretically[14,15] and experimentally[15–17] for the special case in which the wave function is completely confined to the structure's interior. Current experiments of interest on these

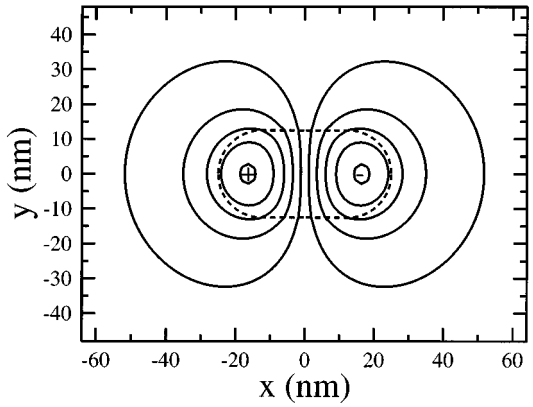

FIG. 1. Contour plot of the first excited bound electronic state of a stadium-shaped structure whose shape is shown by the dashed line. The potential offset is taken to be 10 meV here. Note that this wave function is antisymmetric with respect to reflection through the $x=0$ plane.

shapes have involved electrons on metal surfaces[16] or microwaves in thin cavities.[15,17] In the case of a thin microwave cavity surrounded by metal, a one-to-one correspondence can be drawn between Maxwell's equations and Schrödinger's equation,[17–19] so the eigenfrequencies derived from microwave experiments are simply related to the electronic energies of a two-dimensional quantum dot having the same shape and infinite barriers. The vertical component of the electric field (the square of which can be measured readily) in a microwave cavity is the analog of the wave function in Schrödinger's equation.

It is well known that the states of the stadium structure are nonseparable, and accordingly this shape is of current interest in the study of the onset of chaos and related topics.[14,15] It is worth noting that all previous calculations for this system treated the particle as being completely confined to the interior, whereas in order to study electrons in semiconductor nanostructures we need to allow the particle to tunnel into the classically forbidden (barrier) region. Our ability to implement the BEM for the stadium is an indication of the flexibility of this method. For the purposes of the present discussion, this shape represents either the cross section of a quantum wire or the perimeter of a quantum dot with a growth axis perpendicular to it. These structures are motivated by GaAs nanostructures and we take the electron mass to be 0.0665 in both materials. Table II and Figs. 1 and 3 are motivated by quantum dots that exist within quantum wells. These dots are formed by slight variations in the well width,[20] giving rise to a small potential offset, which we take here to be 10 meV. This choice of band offset results in a structure having only two bound states. The fact that the wave function of the first excited state, plotted in Fig. 1, is only weakly bound to the well region would require a large unit cell if a finite-difference or finite-element method were used to calculate this state, owing to the fact that these latter methods require the wave function to be completely contained within an artificial two-dimensional box.

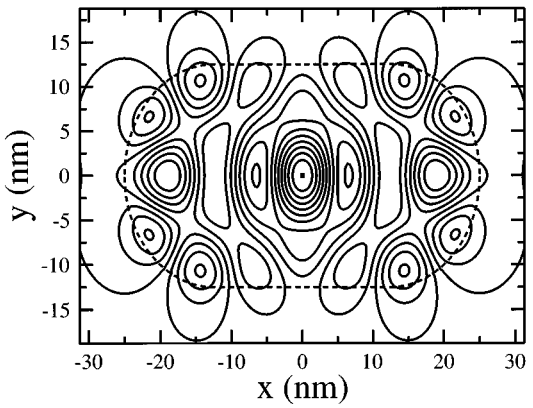

FIG. 2. Contour plot of an excited electronic state of a stadium-shaped structure (dashed line) whose potential offset we take here to be 190 meV. The energy of the bound state is 184.4 meV.

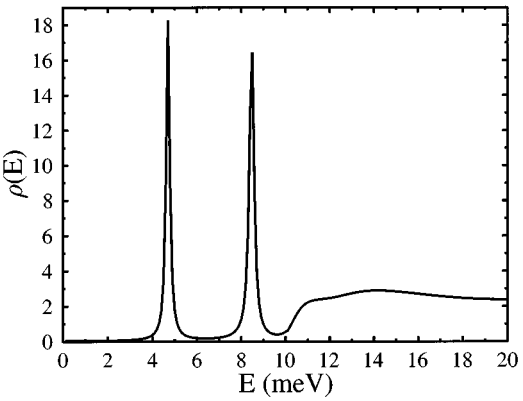

FIG. 3. Spectral density of a 25×50 nm^2 stadium-shaped structure whose potential offset is taken here to be 10 meV. The peaks give the positions of the two bound states and the continuum begins at 10 meV. The bound-state energies of this system are tabulated in Table II, and the wave function of the first excited state is given in Fig. 1. For purposes of presentation we have set $\mathrm{Im}(E) \approx 0.1$ meV.

In Table II the convergence of the energies of the two bound states of this stadium structure with a 10-meV potential offset are given. The energy of each of these states is an appreciable fraction of the potential offset of 10 meV and as a result these bound states have a spatial extent well beyond the nanostructure, as seen in Fig. 1 for the first excited state. From the results in Table II it can be seen that the energies of these states converge well with a modest number of boundary elements $\mathcal{N}$ contained in the irreducible surface, which for this system is one-quarter of the perimeter. In fact, it is seen that the relative error of the calculated energy is $O(\mathcal{N}^{-2})$.

In Fig. 3 the spectral density of the system with a 10-meV barrier offset is given. Note the two peaks for the two bound states near 4.8 and 8.6 meV. For purposes of presentation we have set $\mathrm{Im}(E) \approx 0.1$ meV and therefore the bound states have corresponding widths. For energies above 10 meV the onset of a continuum of states is seen.

In Fig. 2 the same stadium shape is considered with a larger potential offset of 190 meV, which is motivated by a quantum wire of GaAs embedded in $\mathrm{Al}_x\mathrm{Ga}_{1-x}\mathrm{As}$. An example of a highly excited bound state that has an energy slightly below this threshold is shown there. This state ex-

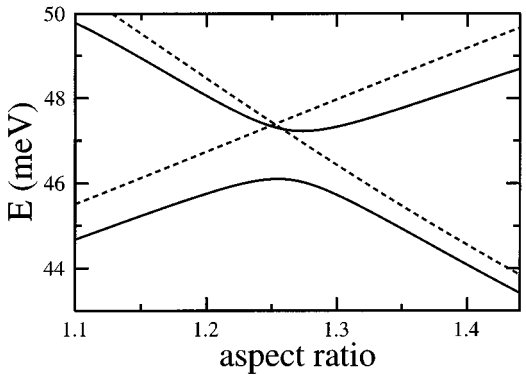

FIG. 4. Plot of the shape dependence of the energies of a rectangular quantum dot for the two particular electronic states discussed in the text. The band offset is here taken to be 50 meV and the dot area to be 1150 nm^2. The dashed lines indicate the energies calculated assuming a separable form for the wave functions and the solid lines are our exact results. The aspect ratio is the ratio of the rectangle's length to its width.

hibits a considerable number of nodes. The numerical calculation of this state, however, requires only approximately $\mathcal{N}=50$ boundary elements in the irreducible perimeter. This example shows that the BEM is efficient and effective in treating highly excited bound states of nanostructures. By comparison, calculations for such a state using a finite-difference method would require $O(\mathcal{N}^2)=O(2500)$ mesh points.

B. Rectangle

In this subsection we consider a rectangular shape whose area is the same as that considered for the stadium in the preceding subsection and whose band offset is taken to equal 50 meV. Although states completely confined within a rectangular shape are separable, states that are partially confined to a rectangle or completely or partially excluded from a rectangle are *not* separable. The nonseparability of this system can be understood most easily by using Cartesian coordinates, in which case Schrödinger's equation separates, but the boundary conditions do not. Hence the states not completely confined to a rectangle cannot be characterized by an ordered pair of quantum numbers, one for the confinement number (n_x) in the x direction and one for the confinement number (n_y) in the y direction. As an illustration of the qualitative importance of this nonseparability, the energies of two bound states of a rectangle having a fixed area but a varying aspect ratio (ratio of length to width) are shown in Fig. 4. If a separable approximation is made for these states' wave functions, then the $(n_x,n_y)=(1,2)$ state and the $(n_x,n_y)=(3,0)$ state are accidentally degenerate when the aspect ratio equals approximately 1.25. However, when the energies are calculated exactly using the BEM, they are seen to exhibit an avoided crossing instead. The extent of the deviations from a simple separable approximation are seen in Fig. 4.

Results for the scattering of an electron from such a rectangle, whose dimensions are 24 × 48 nm^2, are shown in Figs. 5 and 6. The differential scattering cross sections for a 5-meV electron that impinges upon the rectangle from two

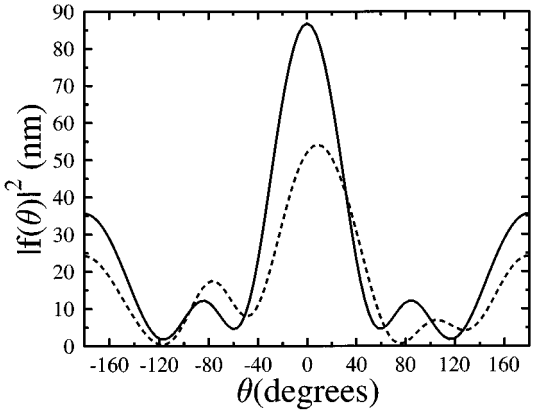

FIG. 5. Results for the scattering of an electron from a rectangular quantum dot having dimensions of 24 × 48 nm^2 and a band offset of 50 meV. Plot of the angle dependence of the differential cross section $|f(\theta)|^2$ for an electron scattering from a rectangular quantum dot, for an incident electron that moves parallel to the rectangle's long axis (solid curve) or along its diagonal (dashed curve). The electron energy is taken here to be 5 meV.

different angles are shown in Fig. 5. The energy dependence of the total scattering cross section σ for an electron that travels initially parallel to the long axis of the rectangle is shown in Fig. 6. The result for the Born approximation, which can be calculated for this geometry and equals the exact result for high E, as expected, is also displayed in this figure. As a check of the correctness of our calculation of the total cross section σ $[\equiv\int d\theta|f(\theta)|^2]$, we also calculated this quantity using the optical theorem, which relates σ to the forward-scattering amplitude. In two dimensions, the optical theorem says that $\sigma=2\sqrt{\pi/k_i}\,\mathrm{Im}[(1-i)f(\theta=0,\overline{k_i})]$. We have used the BEM to calculate each side of this equation independently and the agreement is perfect in the limit of large $\mathcal{N}$.

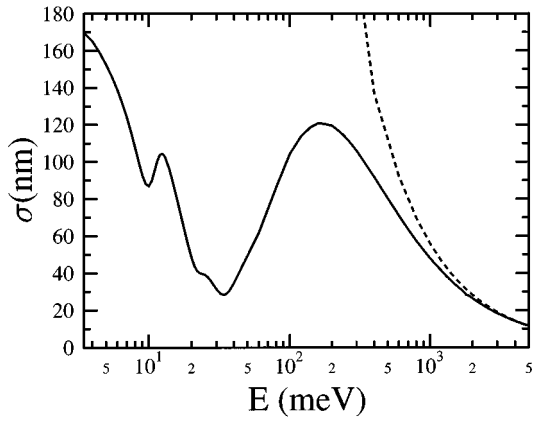

FIG. 6. Results for the scattering of an electron from a rectangular quantum dot having dimensions of 24 × 48 nm^2 and a band offset of 50 meV. Plot of the energy dependence of the total scattering cross section for an electron that moves initially parallel to the rectangle's long axis, calculated using the exact formulation presented in this paper (solid line) and using the Born approximation (dashed curve).

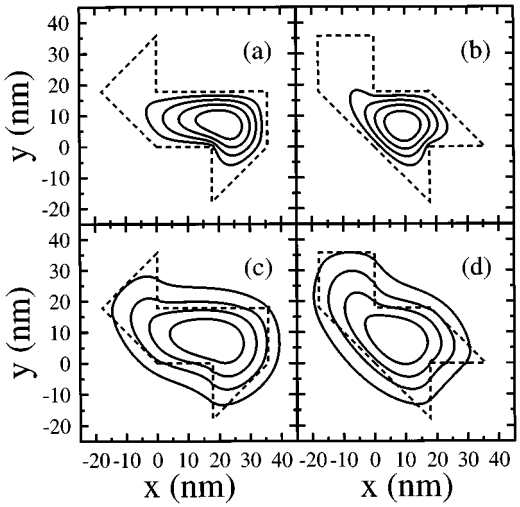

FIG. 7. Results for the ground electronic states of isospectral cavities. The electron mass is taken to be 0.0665. Contour plots of the wave functions of cavities 1 and 2 are respectively shown in (a) and (b) for the case of an infinite band offset. The cavity outlines are indicated by dashed lines. Contour plots of the same states, but for the band offsets having the finite value of 20 meV, are shown in (c) and (d).

C. Isospectral shapes

The extent to which knowledge of the size and shape of a nanostructure can be obtained from spectroscopic results such as photoluminescence data is of fundamental interest. This question is related to a mathematical problem of current interest, which is paraphrased by the question, ''Can one hear the shape of a drum?''[21] That is, can one determine the shape of a drumhead from a knowledge of all of its eigenfrequencies? In recent mathematical[22] and experimental[19] studies of a particular set of shapes known as ''isospectral shapes'' this question has been answered in the negative. The experiments, however, were done in thin metal microwave cavities. The analogous case for nanostructures involves electrons that are forbidden from tunneling out of the structures' interiors.

In the present work we are interested in this example as it relates to the question of determining shapes and sizes of realistic nanostructures from spectroscopic data. An example of one pair of such isospectral shapes is shown by the dashed lines in Figs. 7(a)–7(d). Each one of the pair is composed of seven isosceles right triangles. The shapes have equal areas and equal circumferences. For comparison, we choose the areas of these shapes to equal those of the others studied in Secs. VI A and VI B. The electronic ground-state wave functions for the case of no tunneling into the barriers are shown in Figs. 7(a) and 7(b).[23] Although the wave functions differ for the two structures the energies are identical, which is consistent with the results noted above.[19,22] For many realistic nanostructures, however, carrier tunneling must be included. Results for a finite potential barrier equaling 20 meV are shown in Figs. 7(c) and 7(d). Tunneling into the barriers is found to decrease the energies, of course. More importantly, the eigenenergies of the two structures are no longer identical in the presence of tunneling. The band-offset dependence of the three lowest energies of the two structures

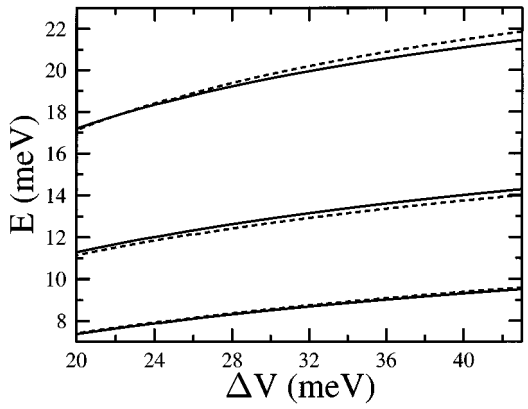

FIG. 8. Results for the lowest three electronic states of isospectral cavities. The electron mass is taken to be 0.0665. The band-offset dependence of the energies of the ground, first excited, and second excited states are shown for cavity 1 (solid line) and cavity 2 (dashed line). The energies of these three states for the case of infinite offset are 18.3, 26.3, and 37.2 meV.

are shown in Fig. 8. It is worth noting that the differences between the energies for the two structures are small even when the eigenenergy is a substantial fraction of the band offset. This suggests that it will be difficult to extract information about the size and shape of realistic nanostructures based solely on spectroscopic data.

D. Lithographically formed structures

In Figs. 9–11 we show examples of the results of calculations of localized and extended states using the BEM that have helped to elucidate experimental results for two lithographically formed quantum-wire structures of current interest. We have studied in Ref. 24 the optical properties in modulated barrier quantum wires formed by selectively etching an overlayer of wider-band-gap material from a quantum well. In Fig. 9 the ground-state wave function of a GaAs/$In_{0.10}Ga_{0.90}$/GaAs modulated barrier quantum wire is shown. That this structure is a nonseparable system can be seen, for example, by noting the extent to which the wave function moves more deeply into the GaAs substrate for narrower wires. The relatively large penetration of the wave function into the GaAs substrate on the side away from the vacuum regions is especially significant and we have found it to be

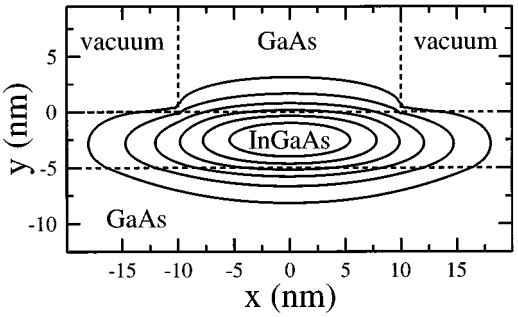

FIG. 9. Contour plot of the ground-state wave function of an electron in a GaAs/$In_{0.10}Ga_{0.90}$As/GaAs modulated barrier quantum wire corresponding to those discussed in Ref. 24.

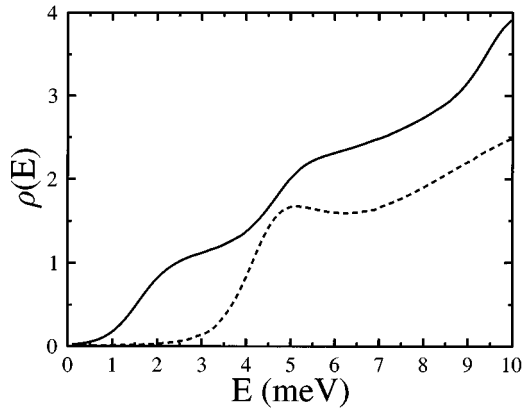

FIG. 10. Results for InP/$In_{0.53}Ga_{0.47}As$/InP deep-etched quantum wires corresponding to those discussed in Ref. 25. The weighted spectral density as a function of energy is given for a 66-nm-wide wire (solid line) and for a 34-nm-wide wire (dashed line).

important in understanding quantitatively the wire width dependence of the energies of the bound states.[24]

In the work in Ref. 25 the photoluminescence rise time of deep-etched InP/$In_{0.53}Ga_{0.47}As$/InP quantum-wire structures was observed to exhibit what appeared to be a barrier for the transport of carriers from the InP substrate into the $In_xGa_{1-x}As$ wire even though no physical barrier was present. In Fig. 10 the spectral density of a system consisting of the InP substrate plus the InP material below a 34-nm $In_xGa_{1-x}As$ wire is shown. It should be noted that the narrower-gap $In_xGa_{1-x}As$ quantum wire is located near the top of the pedestal-like InP structure in Fig. 11. The spectral density is evaluated in the narrow region leading to the $In_xGa_{1-x}As$ wire. It is seen that there is a nonzero spectral density for all energies down to zero, but that there is a fairly abrupt increase of the spectral density for energies increasing above the energy corresponding roughly to the lowest bound state of the vacuum/InP/vacuum quantum-well system. This increase in the spectral density accounts for the appearance of an effective barrier observed in the experiments for temperature-dependent transport from the substrate.[25] Typical wave functions for energies below and above this threshhold are shown respectively in Figs. 11(a) and 11(b). There it is seen that the latter has more amplitude in the region near the wire. Note that both of these wave functions are parts of the continuum that extends throughout the substrate region.

E. Arrays of antidots

In Figs. 12 and 13 we illustrate calculations for a model of a system of four antidots. A single antidot has a repulsive potential that binds no states, but arrays of antidots can give rise to interesting dynamical behavior owing to successive collisions between the electron and neighboring antidots. The electronic properties of such systems have been of particular interest in interpreting quantum beats in magnetotransport and related phenomena.[26] For an array of four antidots, this interesting behavior amounts to an electron's being resonantly localized by the combination of four repulsive potentials.

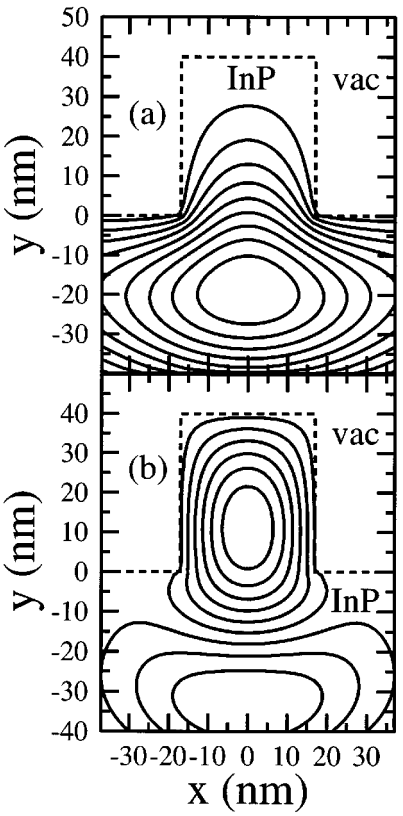

FIG. 11. Results for a 34-nm InP/$In_{0.53}Ga_{0.47}As$/InP deep-etched quantum wire corresponding to those discussed in Ref. 25. Contour plot of an electronic wave function for (a) $E=2$ meV and (b) $E=5$ meV.

Here we will use the BEM to illustrate results for the states of such systems, which form a continuum. We consider a system in which electrons move effectively in a two-dimensional plane in the presence of four antidots as shown in Figs. 12(a) and 12(b). The antidots are taken to circular disks of 100 nm diameter, centered on the corners of a square of 150 nm sidelength, with a potential barrier of 10 meV for electron penetration into the antidots, and the electron mass is taken to be 0.0665. Note that the area of the region encircled by the antidots is larger than, but on the same order as, the area of the shapes considered in Secs. VI A–VI C.

Figure 13 shows the spectral density of this system. All of the states of this system are part of a continuum. Most of these are states in which the carriers can be thought of as scattering from the group of four antidots, which gives the continuous spectral density. In addition, however, there are peaks at approximately 0.6, 1.3, and 3.2 meV, which correspond to resonance states in which the carrier exists preferentially within the region of the four antidots. For the case of no tunneling into the antidots, such resonances have been interpreted as quantum-mechanical ''scars'' of unstable classical orbits.[27] The inverse of the peak width provides a measure of the lifetime of localized states, when viewed in the time domain. In Fig. 12(a) we show the wave function of the 0.6-meV resonance. There it is seen that, although the state exists in the continuum, its wave function is preferentially located in the region of the four antidots. Note that this lowest-energy resonance is symmetric about four antidots, as expected. The peak at 3.2 meV corresponds to a state that is

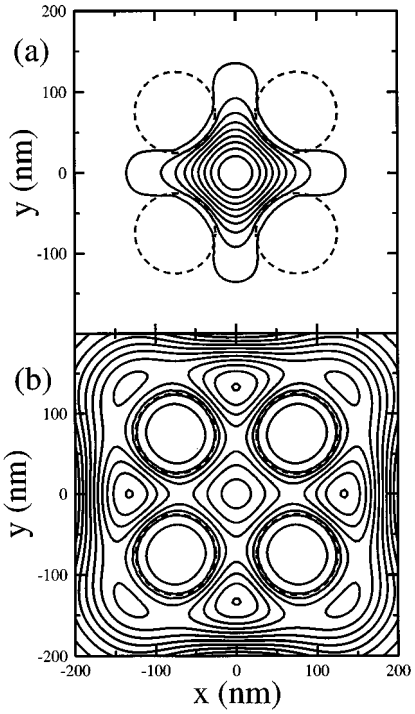

FIG. 12. Results for the electronic states of a system consisting of four antidots. Note that all states are continuum states. Contour plots of electronic states having (a) $E=0.6$ meV, which is preferentially located in the region of the four dots, and (b) $E=0.7$ meV, which tends to scatter from the region of the four dots.

antisymmetric with respect to reflection through either the x axis or the y axis. The peak at 1.3 meV consists of two degenerate resonances, the wave function for each of which is antisymmetric with respect to reflection in one direction and symmetric with respect to reflection in the orthogonal one. In Fig. 12(b) a wave function of a 0.7-meV state is shown. This state is nonresonant and has the appearance of being scattered by the group of four antidots.

VII. SUMMARY

In the present work we have developed a boundary-element method for calculating the electronic properties of nanostructure systems of arbitrary geometries and effective dimensionalities. Green's function techniques have been used to develop the formalism, and the resulting integral equations are discretized and solved by matrix techniques. Results are given for bound and continuum states, for the wave functions, for the spectral density functions, and for scattering cross sections. In effect, this integral equation approach reduces a problem involving a differential equation and boundary conditions in d independent variables to an integral equation in $d-1$ independent variables, which leads to its efficiency. A number of illustrative examples taken from nanostructural systems of current interest are given here. It should be noted that this approach is especially effective for calculating the properties of highly excited states with numerous nodes and also for handling geometries with sharp corners and unusual shapes, for which other methods often have difficulties.

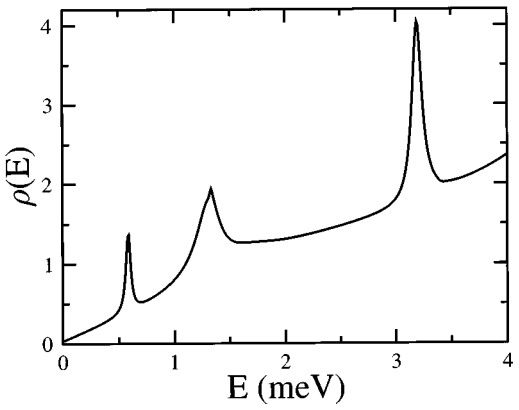

FIG. 13. Results for the electronic states of a system consisting of four antidots. Note that all states are continuum states. Spectral density as a function of energy. The peaks correspond to resonances that are preferentially located in the region surrounded by the four antidots and the background continuum is associated with completely free states impinging on the exterior perimeter of the antidots.

ACKNOWLEDGMENTS

This work was supported in part by the U. S. Office of Naval Research. T.L.R. gratefully acknowledges the financial support of the Alexander von Humboldt Foundation and the hospitality of the Max-Planck Institut für Festkörperforschung, Stuttgart. P.A.K. gratefully acknowledges helpful conversations with A. Kudrolli, S. Sridhar, and F. Robicheaux. T.L.R. and P.A.K. gratefully acknowledge helpful conversations with A. Forchel and the members of his group at the University of Würzburg.

*Electronic address: pknipp@pcs.cnu.edu
†Electronic address: reinecke@estd.nrl.navy.mil
‡Permanent address.

[1] See, e.g., Lin-Wang Wang and Alex Zunger, in *Nanocrystalline Semiconductor Materials*, edited by P. V. Kamat and D. Meisel (Elsevier, New York, 1996).
[2] Arvind Kumar, Surf. Sci. **263**, 335 (1992); V. V. Paranjape, SPIE Quantum Well Superlatt. Phys. III **1283**, 287 (1990).
[3] See, for example, L. R. Ram-Mohan and J. R. Meyer, J. Nonlin. Opt. Phys. Mater. **4**, 191 (1995).
[4] P. A. Knipp and T. L. Reinecke, Phys. Rev. B **45**, 9091 (1992).
[5] P. A. Knipp and T. L. Reinecke, Phys. Rev. B **46**, 10 310 (1992).
[6] P. A. Knipp and T. L. Reinecke (unpublished).
[7] P. A. Knipp and T. L. Reinecke (unpublished).
[8] Erik Ivar Fredholm, *Sur un Nouvelle Methode pour la Resolution du Probleme de Dirichlet* (Ofr. Fork. Akad., Stockholm, 1900).
[9] George R. C. Tai and Richard Paul Shaw, J. Acoust. Soc. Am. **56**, 796 (1974); Yi Yan, SIAM J. Numer. Anal. **31**, 477 (1994).
[10] See, for example, G. Bastard, *Wave Mechanics Applied to Semiconductor Heterostructures* (Wiley, New York, 1988), Chap. III.
[11] The discontinuities in $\mathcal{V}(\mathbf{r})$ and $m(\mathbf{r})$ at interfaces separating different regions are the cause of serious convergence difficulties when plane-wave expansions are used to approximate the wave function.
[12] R. J. Riddell, Jr., J. Comput. Phys. **31**, 21 (1979).
[13] P. A. Knipp and T. L. Reinecke, Phys. Rev. B **48**, 18 037 (1993).

[14] R. D. Taylor and P. Brumer, Faraday Discuss. Chem. Soc. **75**, 170 (1983); Eric J. Heller, Phys. Rev. Lett. **53**, 1515 (1984); P. W. Brouwer and C. W. J. Beenakker, Phys. Rev. B **50**, 11 263 (1994).

[15] J. Stein, H.-J. Stöckmann, and U. Stoffregen, Phys. Rev. Lett. **75**, 53 (1995).

[16] E. J. Heller, M. F. Crommie, C. P. Lutz, and D. M. Eigler, Nature **369**, 464 (1994).

[17] H.-J. Stöckmann and J. Stein, Phys. Rev. Lett. **64**, 2215 (1990); H.-D. Gräf *et al.*, *ibid.* **69**, 1296 (1992); H. Alt *et al.*, *ibid.* **74**, 62 (1995).

[18] J. D. Jackson, *Classical Electrodynamics* (Wiley, New York, 1975), Chap. 8.

[19] S. Sridhar and A. Kudrolli, Phys. Rev. Lett. **72**, 2175 (1994).

[20] D. Gammon, E. S. Snow, and D. S. Katzer, Appl. Phys. Lett. **67**, 2391 (1995).

[21] M. Kac, Am. Math. Mon. **73**, 1 (1966).

[22] Carolyn Gordon *et al.*, Bull. Am. Math. Soc. **27**, 134 (1991); S. J. Chapman (unpublished).

[23] For the case of no tunneling into the barrier, these wave functions have also been calculated using a different method by Hua Wu *et al.* [Phys. Rev. E **51**, 703 (1995)].

[24] Ch. Gréus, L. Butov, F. Daminger, A. Forchel, P. A. Knipp, and T. L. Reinecke, Phys. Rev. B **47**, 7626 (1993); Ch. Gréus, R. Spiegel, P. A. Knipp, T. L. Reinecke, F. Faller, and A. Forchel, *ibid.* **49**, 5753 (1994).

[25] F. Kieseling, W. Braun, K. H. Wang, A. Forchel, P. A. Knipp, T. L. Reinecke, Ph. Pagnod-Rossiaux, and L. Goldstein, Phys. Rev. B **52**, R11 595 (1995).

[26] E. Vasiliadou *et al.*, Phys. Rev. B **52**, R8658 (1995).

[27] P. Gaspard *et al.*, Phys. Rev. E **50**, 2591 (1994).